J. Micro. and Elect. Pack. **5**, 101−106 (2008).

Broadband Dielectric Characterization of Aluminum Oxide (Al_2O_3)

Khalid Z. Rajab[1,2], Mira Naftaly[3], Edmund H. Linfield[3], Juan C. Nino[4], Daniel Arenas[5], David Tanner[5], Raj Mittra[2], and Michael Lanagan[1]

[1] Materials Research Laboratory, Pennsylvania State University, University Park, PA 16802, USA
[2] Department of Electrical Engineering, Pennsylvania State University, University Park, PA 16802, USA
[3] Department of Electronic and Electrical Engineering, University of Leeds, Leeds LS2 9JT, UK
[4] Materials Science and Engineering Department, University of Florida, Gainesville, FL 32611, USA
[5] Physics Department, University of Florida, Gainesville, FL 32611, USA

Abstract

Applications for low temperature co-fired ceramics (LTCC) and high temperature co-fired ceramics (HTCC) are advancing to higher frequencies. In order to design ceramic microsystems and electronic packages, the electrical properties of materials must be well characterized over a broad frequency range. In this study, the dielectric properties of commercial Aluminum Oxide (Al_2O_3) with different glass loadings have been characterized using three different measurement techniques: the split-post cavity, terahertz (THz) time-domain spectroscopy, and Fourier transform infrared spectroscopy (FTIR). Specifically, the dielectric properties will be characterized from 10 GHz to infrared frequencies. A split-post cavity was employed for determination of dielectric properties in the 10 GHz range. A broadband terahertz (THz) spectroscopy technique was used to characterize the specimens using measured time-domain transmission data. The dielectric constant and loss were extracted from the sample's frequency-domain transmission characteristics, providing data between 100 GHz to 2 THz. Additionally, Fourier transform infrared spectroscopy (FTIR) was used to characterize the samples from ~33 to 3300 cm^{-1} (~ 1THz – 100 THz). The measurements from the three techniques are compared, and dielectric constant and loss data will be presented for commercial and experimental ceramic systems from 10 GHz to infrared frequencies.

Key words:

1. Introduction

Dielectric properties of ceramic materials are generally characterized by using a parallel plate capacitor technique at frequencies below 10 MHz. In the GHz range, a variety of characterization methods are employed and method selection depends upon the sample shape and dielectric properties. Resonant techniques are useful for low loss dielectric specimens *(tan $\delta < 10^{-2}$)*. The split-cylinder technique [1,2] is a commonly used method for dielectric characterization of thin, flat samples in the microwave regime, due to its accurate determination of permittivities and loss tangents of low-loss dielectrics. Transmission characterization methods are important for broadband dielectric property determination. Recently, with the development of new and higher-power broadband sources [3] for operation at terahertz frequencies (loosely defined as 0.1 to 10 THz or 100 to 10^4 GHz), many new applications are being developed at these frequencies, including the demonstration of THz detection of single base-pair differences in femtomolar concentrations of DNA [4], tomographic imaging [5,6], investigation of molecular vibrational modes [7,8], and the characterization of thin- [9] and thick-film [10] ceramics. With the lower end of the terahertz frequency band closely matching with the resonant frequency of the split-cylinder technique, a comparison between the results from the characterization of low-loss ceramics with these techniques should provide insight into the suitability of the inherently broadband terahertz spectroscopy measurements for these dielectric characterizations.

Ceramic specimens are characterized at the 10 GHz range using a split-cylinder technique, in the 10 GHz to 1 THz range using a broadband time-domain spectroscopy system [11,12], and at the 1 THz to 100 THz range using a Fourier transform infrared spectroscopy (FTIR) system [13]. The

permittivities and loss tangents are found using the three different techniques.

2. Experimental

2.1 Samples

The two samples are composed of commercial grade Alumina mixed with glass. The first sample is 96% Alumina and 4% glass, and the second sample is composed of 99.6% Alumina and 0.4% glass. The thicknesses of the samples are 620 μm and 660 μm respectively.

2.2 Split-cylinder technique

The complex permittivity of the ceramics was characterized at microwave frequencies using a split-cavity technique [1,2]. The fixture consists of a fixed lower cavity, and an upper cavity that is lowered to sandwich the dielectric in-between. An HP 8510C network analyzer is used to obtain the transmitted frequency spectrum, and the TE_{011} resonant mode of the system is used to obtain the complex permittivity of the enclosed dielectric.

2.3 Pulsed THz transmission measurements

A diode laser pumped Ti:Sapphire laser emits 60 μs pulses at a center wavelength of 790 nm, operating at 80 MHz. The beam is split so that 90% of the intensity is used as a pump beam for THz generation, with the other 10% used as a probe beam for detection. THz generation was provided by excitation of a biased GaAs photo-conductive aperture antenna, with the THz pulses collimated and focused by a series of off-axis parabolic mirrors through the sample, and onto a 1 mm thick ZnTe crystal. The frequency dependent complex permittivity is obtained from the frequency spectrum, which is found by performing a Fast Fourier Transform (FFT) on the measured time-domain data.

2.4 IR reflectivity measurements

Frequency dependant reflectivity was obtained using a Fourier transform spectrometer (Bruker IFS 113v) in conjunction with a Si bolometer (over 30 – 700 cm^{-1}) and a DTGS detector (over 650 – 5000 cm^{-1}). The reflection stage provided an angle of incidence of about 15° for the light. The frequency dependant complex permittivity is then found by fitting to a model dielectric function [13].

3. Results and Discussions

3.1 Split-cylinder microwave characterization

Complex permittivity measurements at microwave frequencies (~17GHz) of the two Alumina samples are determined using the split-cavity technique [1,2], with results shown in Table I. The 99.6% Alumina composition has a higher permittivity and lower loss than the 96% Alumina at these frequencies.

Table I: Relative permittivity and loss tangent of Alumina samples, as measured with the split cavity.

Sample	Split Cylinder (17GHz)	
	Permittivity, ε'	Loss tangent, tanδ
96% Alumina	9.164	7.4×10^{-4}
99.6% Alumina	9.424	3.1×10^{-4}

3.2 Terahertz transmission spectra

Terahertz time-domain spectroscopy relies on obtaining the transmitted frequency spectrum through the sample. Reference data is initially obtained, in the time domain, without a sample in the fixture between the transmitter and the receiver. The experiment is then repeated with the sample in place, with results for all of the specimens shown in Fig. 1. Once the data has been transformed to the frequency domain using an FFT, the complex ratio of the sample spectrum to the reference spectrum, with magnitude shown in Fig. 2, may be used to find the complex permittivity of the sample.

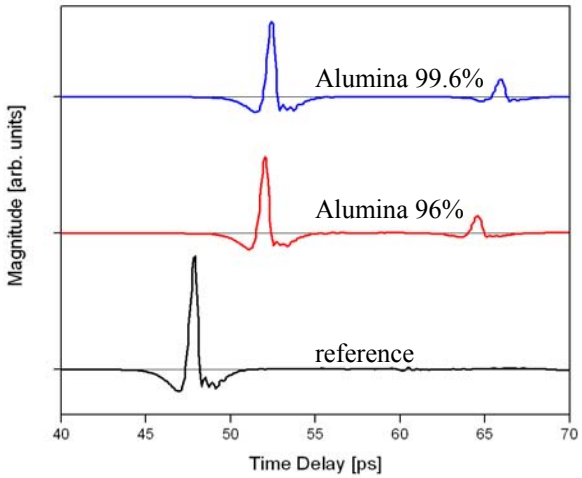

Figure 1: Time domain transmitted signal through a vacuum reference (black –), and Alumina 96% (red –) and 99.6% (blue –). The specimens with greater relative permittivity have longer pulse delays.

The transmission spectra of a sample, along with the reference, may be used to investigate its dielectric properties. Taking into account Fabry-Perot effects through a three-medium sample (with the

outer two mediums being air), the transmission t(ω) may be derived by using the Fresnel formulas:

$$t(\omega) = \frac{T_{sample}(\omega)}{T_{ref}(\omega)} = \frac{\frac{4\tilde{n}}{(\tilde{n}+1)^2}\exp\left(-j\frac{\omega(\tilde{n}-1)d}{c}\right)}{1-\frac{(\tilde{n}-1)^2}{(\tilde{n}+1)^2}\exp\left(-j\frac{2\omega\tilde{n}d}{c}\right)}, \quad (1)$$

where $\tilde{n} = n - j\kappa$ is the complex index of refraction of the sample, d is the thickness of the sample, c is the speed of light in a vacuum, and t(ω) is the ratio of the transmission spectrum with the sample to the spectrum without the sample. $\tilde{n}$ may be solved for numerically, providing the complex index of refraction as well as the complex permittivity which, for a non-magnetic material, is defined as:

$$\varepsilon(\omega) = \varepsilon'(\omega) - j\varepsilon''(\omega) = \sqrt{\tilde{n}(\omega)}\,. \quad (2)$$

Subsequently, the loss tangent is calculated as:

$$\tan\delta = \frac{\varepsilon''}{\varepsilon'}\,. \quad (3)$$

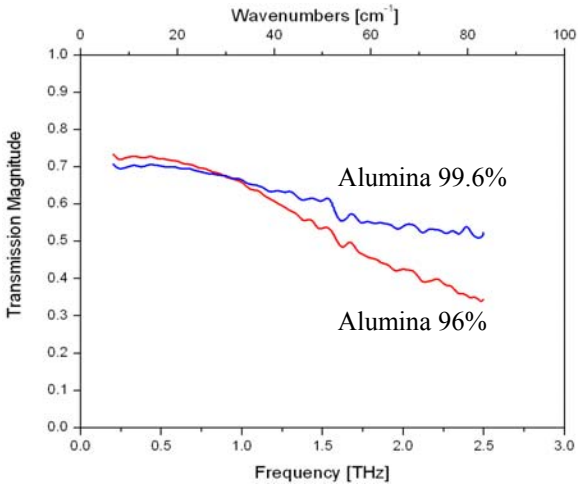

Figure 2: Frequency domain transmission spectrums through Alumina 96% (red –) and 99.6% (blue –) as measured using terahertz time-domain spectroscopy.

However, eq. (1) relies on numerical techniques to solve for the complex index of refraction. Additionally, the equation includes all temporal echoes caused by reflections in the slab leading to time-delayed transmitted pulses. Theoretically, all pulses must be accounted for in the Fourier-transformed spectrum. In practice, a sufficient number of pulses must be measured in order to account for a significant portion of the total transmitted power is accounted. This may require a time-domain measurement that is longer than is practical, and may include interference caused by reflections from instrumentation. This, along with the numerical techniques required to find a solution, makes eq. (1) impractical for complex refractive index extraction.

A more efficient technique that also relies on the transmission spectra, solves for the refractive index in terms of two materials with different thicknesses (where the thinner material can be taken to have zero thickness, *i.e.* the reference spectrum). The solution has been derived for each echo and for the case of the directly transmitted signal [14], in which case all subsequent echoes may be neglected. Experimentally, the sample must be selected so that there is sufficient time-delay between the echoes, in order for them to be analyzed independently. For the case of the directly transmitted signal, the real index of refraction can be found from the phase change between the reference spectrum and the sample spectrum, as:

$$n = 1 + \frac{c\cdot(\phi_{sample} - \phi_{ref})}{\omega\cdot d}, \quad (4)$$

where $(\phi_{sample} - \phi_{ref})$ is the phase difference between the sample spectrum and the reference spectrum. Similarly, the imaginary index of refraction may be found from the previous result, as well as the magnitude of the transmission, as:

$$\kappa = \frac{c}{\omega\cdot d}\ln\left|\frac{4n}{(1+n)^2}\cdot\frac{A_{ref}(\omega)}{A_{sample}(\omega)}\right|, \quad (5)$$

where A_{ref} and A_{sample} are the magnitudes of the reference and sample transmission spectra, respectively. The absorption can then be found, and is defined by:

$$\alpha = \frac{2\omega\kappa}{c}\,. \quad (6)$$

3.3 IR reflectivity spectra

At higher frequencies, the complex permittivity can be determined using the reflectivity

spectra $R(\omega)$, shown in Fig. 3, measured using an FTIR system. A model dielectric function can be fit using the polar phonon modes measured plus a high-frequency permittivity ε_∞ [13]:

$$\varepsilon(\omega) = \varepsilon_\infty + \varepsilon_{ph} = \varepsilon_\infty + \sum_{i=1}^{n} \frac{\Delta\varepsilon_i \omega_i^2}{\omega_i^2 - \omega^2 - j\omega\gamma_i}, \quad (7)$$

where ε_{ph} is the phonon contribution to the complex permittivity, and ω_i, γ_i, and $\Delta\varepsilon_i$ denote the resonant frequency, the damping coefficient, and the contribution to the dielectric permittivity of the ith phonon mode. Subsequently, the complex index of refraction and the absorption coefficient can be found using (2) and (6). The fitting parameters of the reflectance spectra for Alumina are shown in Table II for the 96% composition, and Table III for the 99.6% composition. ε_∞ of Alumina is 3.1.

Table II: Parameters from the dispersion analysis of the phonon modes in the infrared spectra of Alumina 96%.

Resonant Frequency, ω_0 [cm^{-1}]	Oscillator Strength, $\Delta\varepsilon$	Damping Coefficient, γ [cm^{-1}]
204	1.16	191.8
287	0.16	60.1
346	0.15	50.0
384	0.15	5.2
436	1.60	19.4
501	0.03	8.7
569	0.04	4.7
577	0.58	18.0
601	0.30	33.9
638	0.10	18.8
669	0.32	73.5
751	0.35	97.3
817	0.12	71.2

3.4 Optical constants and material parameters

The real parts of the index of refraction, found from eq. (4), are plotted in Figs. 4 and 5 for the 96% and 99.6% Alumina compositions, respectively, ranging from the microwave single-frequency value obtained at around 17 GHz, through to the broadband values calculated from THz-TDS and FTIR measurements. Similarly, the values of the absorption derived from eqs. (5) and (6), the real part of the relative permittivity obtained from (2), and the loss tangent obtained from (3), are all plotted for the two compositions in Figs. 6 and 7, 8 and 9, and 10 and 11 respectively.

Table III: Parameters from the dispersion analysis of the phonon modes in the infrared spectra of Alumina 99.6%.

Resonant Frequency, ω_0 [cm^{-1}]	Oscillator Strength, $\Delta\varepsilon$	Damping Coefficient, γ [cm^{-1}]
385	0.25	4.1
405	0.63	16.6
435	2.73	4.0
495	0.05	10.9
573	2.60	14.2
633	0.11	7.0
769	0.07	143.6

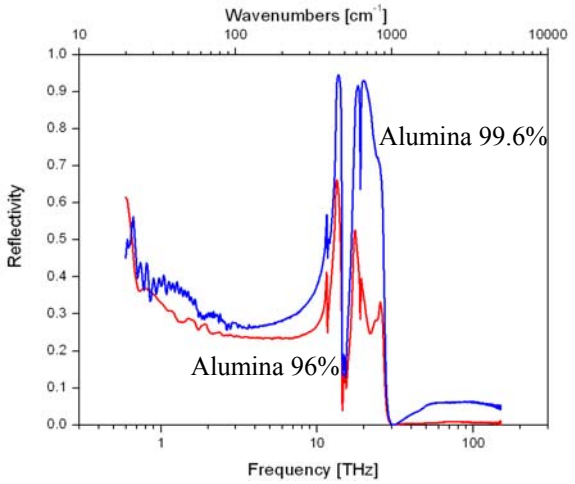

Figure 3: Frequency domain reflectivity spectrums of Alumina 96% (red –) and 99.6% (blue –) as measured using Fourier-transform infrared spectroscopy.

The significantly higher dielectric loss at THz frequencies is consistent with the intrinsic and extrinsic dispersion models. Intrinsic loss is related to infrared lattice modes [15], while extrinsic dielectric loss caused by point defects, stacking faults, and grain boundaries add to the intrinsic high frequency losses. At higher frequencies, i.e. when the condition that $\omega << \omega_1$ is not satisfied, and particularly in the terahertz regime, the constant "Q×f" approximation no longer holds. In particular, it has been shown in [16] and [17] that the many structural and lattice defects in ceramics introduce additional extrinsic losses. For this reason, we would expect the losses measured using THz-TDS to be greater than those found using the IR phonon modes that are measured

by FTIR. This trend is verified by the absorption and loss tangent plots of the 99.6% Alumina. Additionally, the refractive index and the relative permittivity measurements correlate well. The 96% Alumina measurements show a discrepancy between the two measurement techniques that can be further investigated using Kramers-Kronig analysis [18]

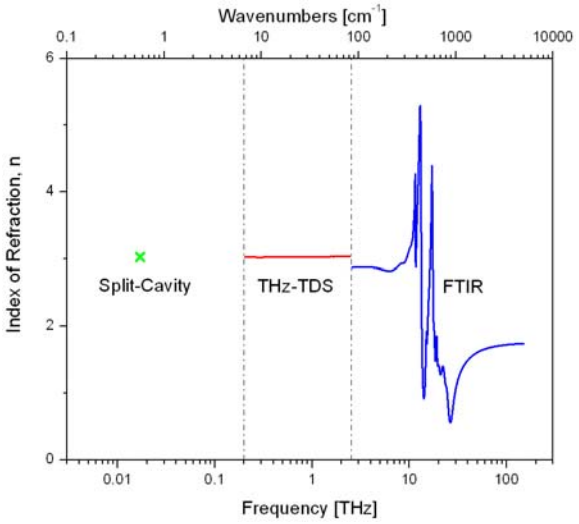

Figure 4: Real index of refraction, n of Alumina 96%, as measured using the split-cavity technique (green ×), terahertz time-domain spectroscopy (red –**)**, and Fourier-transform infrared spectroscopy (blue –).

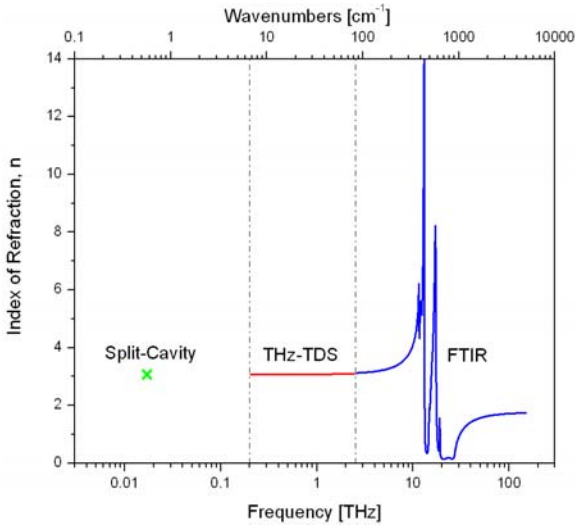

Figure 5: Real index of refraction, n of Alumina 99.6%, as measured using the split-cavity technique (green ×), terahertz time-domain spectroscopy (red –**)**, and Fourier-transform infrared spectroscopy (blue –).

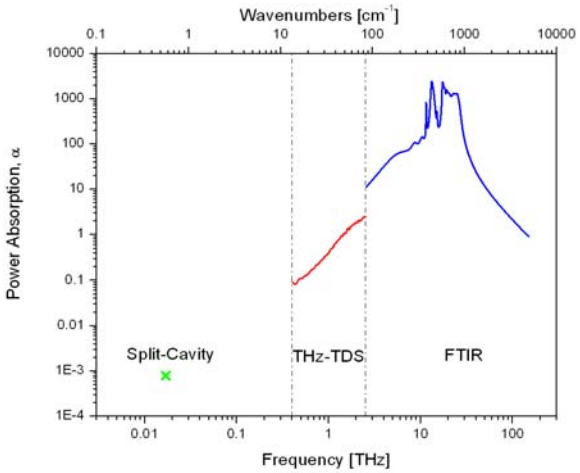

Figure 6: Power absorption coefficient, α of Alumina 96%, as measured using the split-cavity technique (green ×), terahertz time-domain spectroscopy (red –**)**, and Fourier-transform infrared spectroscopy (blue –).

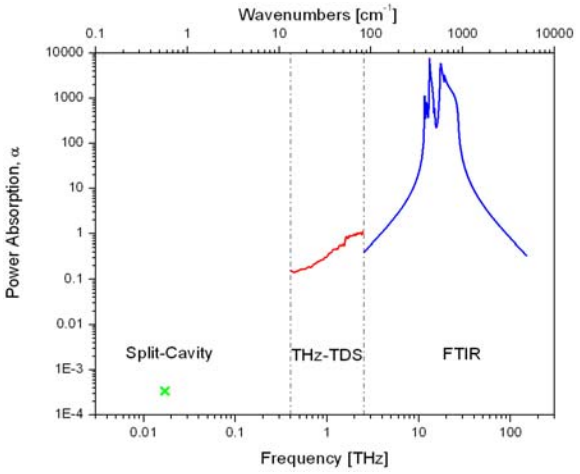

Figure 7: Power absorption coefficient, α of Alumina 99.6%, as measured using the split-cavity technique (green ×), terahertz time-domain spectroscopy (red –**)**, and Fourier-transform infrared spectroscopy (blue –).

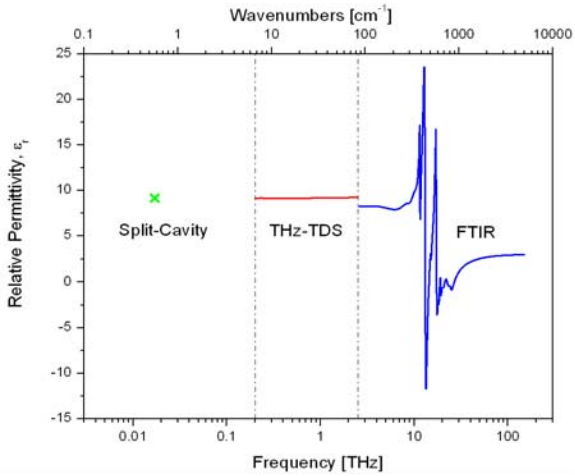

Figure 8: Relative permittivity, ε_r of Alumina 96%, as measured using the split-cavity technique (green ×), terahertz time-domain spectroscopy (red –**)**, and Fourier-transform infrared spectroscopy (blue –).

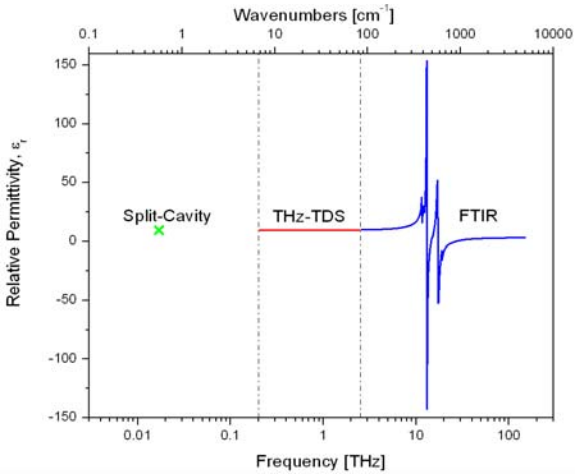

Figure 9: Relative permittivity, ε_r of Alumina 99.6%, as measured using the split-cavity technique (green ×), terahertz time-domain spectroscopy (red –**)**, and Fourier-transform infrared spectroscopy (blue –).

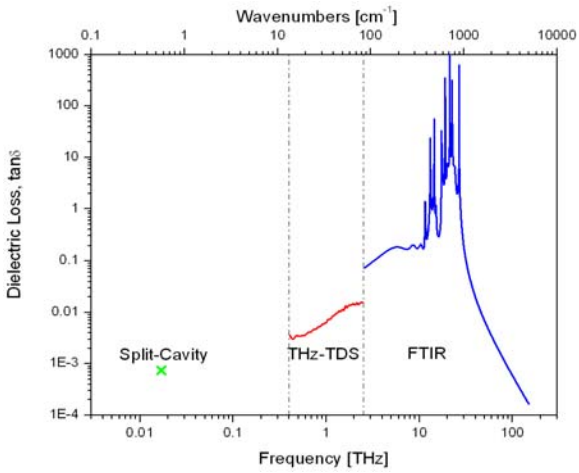

Figure 10: Dielectric loss tangent, tanδ of Alumina 96%, as measured using the split-cavity technique (green ×), terahertz time-domain spectroscopy (red –**)**, and Fourier-transform infrared spectroscopy (blue –).

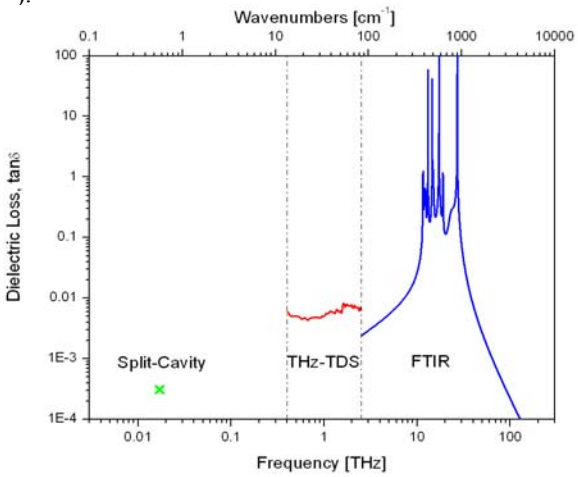

Figure 11: Dielectric loss tangent, tanδ of Alumina 99.6%, as measured using the split-cavity technique (green ×), terahertz time-domain spectroscopy (red –**)**, and Fourier-transform infrared spectroscopy (blue –).

4. Conclusion

Commercial grade Alumina samples mixed with different quantities of glass were characterized for their dielectric properties at both microwave frequencies, using a split-cylinder technique, and terahertz frequencies using time-domain spectroscopy and Fourier-transform infrared spectroscopy. The complex indices of refraction, as well as the relative permittivities and loss tangents were found for the two samples.

The material characteristics obtained by the different techniques agreed well, allowing the characterization of the dielectric properties of the

Alumina compositions over a broad frequency band, ranging from ~10 GHz to ~100 THz.

Acknowledgment:

The authors gratefully acknowledge financial support from the NSF sponsored Center for Dielectric Studies and the Ben Franklin Technology Center.

References

[1] G. Kent, "Nondestructive Permittivity Measurement of Substrates," IEEE Trans. Instrum. Meas., vol. 45, pp. 102-106, Feb. 1996.

[2] M. D. Janezic, and J. Baker-Jarvis, "Full-wave Analysis of a Split-cylinder Resonator for Nondestructive Permittivity Measurements," IEEE Trans. Microwave Theory Tech., vol. 47, no. 10, pp. 2014-2020, Oct. 1999.

[3] B. Ferguson and X.-C. Zhang, "Materials for Terahertz Science and Technology," Nature Materials, vol. 1, pp. 26-33, September, 2002.

[4] M. Nagel, P. Haring Bolivar, M. Brucherseifer and H. Kurz, "Integrated THz Technology for Label-free Genetic Diagnostics," Apply. Phys. Lett., **80**, pp. 154-156, 2002.

[5] B. B. Hu and M. C. Nuss, "Imaging with Terahertz Waves," Opt. Lett., **20**, pp. 1716-1718, 1995.

[6] B. Ferguson, S. Wang, D. Gray, D. Abbott, and X.-C. Zhang, "T-ray Computed Tomography," Opt. Lett., **27**, pp. 1312-1314, 2002.

[7] Y. C. Shen, P. C. Upadhya, E. H. Linfield, and A. G. Davies, "Vibrational Spectra of Nucleosides Studied Using Terahertz Time-domain Spectroscopy," Vibrational Spectroscopy, **35**, pp. 111-114, 2004.

[8] P. C. Upadhya, Y. C. Shen, A. G. Davies, and E. H. Linfield, "Far-infrared Vibrational Modes of Polycrystalline Saccharides," Vibrational Spectroscopy, **35**, pp. 139-143, 2004.

[9] Z. Jiang, M. Li, and X.-C. Zhang, "Dielectric Constant Measurement of Thin Films by Differential Time-domain Spectroscopy," Appl. Phys. Lett. **76**, pp. 3221-3223.

[10] T.-R. Tsai, C.-C. Chi, M.-H. Liang, C.-T. Hu, and I.-N. Lin, "Dielectric Properties of (x) Complex Perovskite Ceramics," Materials Chemistry and Physics, **79**, pp. 169-174, 2003.

[11] M. C. Beard, G. M. Turner, C. A. Schuttenmaer, "Terahertz spectroscopy," J. Phys. Chem. B, 2002, 106, 7146-7159.

[12] P. Y. Han, M. Tani, U. Usami, S. Kono, R. Kersting, X.-C. Zhang, "A direct comparison between terahertz time-domain spectroscopy and far-infrared Fourier transform spectroscopy," J. Appl. Opt., 2001, 89/4, 2357-2359.

[13] M. Chen, D. B. Tanner, and J. C. Nino, "Infrared study of the phonon modes in bismuth pyrochlores," Phys. Rev. B **72**, 054303, 2005.

[14] L. Duvillaret, F. Garet, and J.-L. Coutaz, "Influence of noise on the characterization of noise by terahertz time-domain spectroscopy," J. Opt. Soc. Am. B, vol. 17, no. 3, Mar. 2000.

[15] K. Wakino, M. Murata, and H. Tamura, "Far infrared reflection spectra of $Ba(Zn,Ta)O_3$-$BaZr)_3$ dielectric resonator material," J. Am. Ceram. Soc. **69**, pp. 34-37, 1986.

[16] E. Schlömann, "Dielectric losses in ionic crystals with disordered charge distributions," Phys. Rev., vol. 135, no. 2A, pp. A413-A419, 1964,

[17] H. Tamura, "Microwave dielectric losses caused by lattice defects," J. Eur. Ceram. Soc., vol. 26, pp. 1775-1780, 2006.

[18] F. Wooten, "Optical Properties of Solids", Academic Press, New York, 1972.